Edge-Bridged Tetrahedral Geometry of Five-Coordinate d^0 Complexes, Relatives of the Bent $[MCp_2L_3]$ Family: A Theoretical and Structure-Correlation Study

Thomas R. Ward,*,† Hans-Beat Bürgi,‡ François Gilardoni,§ and Jacques Weber§

Contribution from the Department of Chemistry and Biochemistry and Laboratory of Chemical and Mineralogical Crystallography, University of Berne, Freiestrasse 3, CH-3012 Berne, and Department of Physical Chemistry, University of Geneva, 30 Quai E. Ansermet, CH-1211 Geneva 4, Switzerland

Received July 7, 1997. Revised Manuscript Received October 6, 1997[⊗]

Abstract: The edge-bridged tetrahedral geometry of five-coordinate d^0 complexes $[MD_2L_3]$ with strong π-donors D is analyzed with extended Hückel methodology as well as density functional theory. It is shown that this geometry, also encountered in bent metallocene systems $[MCp_2L_3]$, can be considered as a distortion of a regular trigonal bipyramid arising from a second-order Jahn−Teller distortion of e′ symmetry (in D_{3h}) and corresponds to a deformation along a reversed-Berry pathway. This model was tested with a structure-correlation analysis of all experimentally determined $[MD_2L_3]$ structures, thus allowing a mapping of the reversed-Berry pathway. The catalytic potential of these complexes and their isolobal relationship to $[MCp_2L_3]$ are emphasized.

Introduction

The square pyramid (SPY-5) and the trigonal bipyramid (TB-5) represent prototypical geometries of five-coordinate complexes. These geometries and their interconversion along the Berry pathway as well as the reactivity and catalytic potential of the corresponding compounds have been thoroughly studied, often as a function of the number of metal d electrons.[1−8] This work focuses on the electronic and geometric structure of five-coordinate d^0 complexes.

Considering cyclopentadienyls as 6-electron donors occupying a single coordination site, $[MCp_2L_3]$ complexes are also five-coordinate. However, d^0 $[MCp_2L_3]$ compounds cannot be categorized as either TB-5 or SPY-5. This is illustrated with four examples: $[TaCp_2H_3]$ (**1**) is one of the first structurally characterized $[MCp_2L_3]$ complexes;[9] $[ZrCp_2Cl(\eta^2\text{-}CH_3CO)]$ (**2**) is an early example of an η^2-bound acyl;[10] $[ZrCp_2(\eta^4\text{-}C_4H_6)]$ (**3**) contains a *trans*-coordinated diene,[11,12] and **4** contains a planar four coordinate carbon.[13] Structural features common to these complexes are a bent $\{MCp_2\}$ fragment and a coplanar arrangement of the three ligands L with two acute L−M−L angles. We call this unusual $[MCp_2L_3]$ geometry "edge-bridged tetrahedral", abbreviated as EBT-5. The geometry of these complexes has been rationalized with the help of molecular orbital (MO) theory at various degrees of sophistication.[12,14−19] In all cases, the presence of three low-lying empty orbitals in the *yz* plane sandwiched between both Cp rings has been invoked. These are depicted in Figure 1.

$[MCp_2L_3]$ complexes with their bent $\{MCp_2\}$ fragment not only show unprecedented geometries but also have led to impressive catalytic applications, among them the stereospecific polymerization of α-olefins.[20−22] Although much effort has been invested to improve on existing catalysts,[23−25] most systems still incorporate bent $\{MCp_2\}$ fragments in many disguises.[26−28] It is generally accepted that the transition state for chain propagation involves a five-coordinate geometry (**5**) with an

† Department of Chemistry and Biochemistry, University of Berne.
‡ Laboratory of Chemical and Mineralogical Crystallography, University of Berne.
§ University of Geneva.
⊗ Abstract published in *Advance ACS Abstracts,* December 1, 1997.

(1) Berry, R. S. *J. Chem. Phys.* **1960**, *32*, 933.
(2) Muetterties, E. L.; Guggenberger, L. J. *J. Am. Chem. Soc.* **1974**, *96*, 1748.
(3) Rossi, A. R.; Hoffmann, R. *Inorg. Chem.* **1975**, *14*, 365.
(4) Holmes, R. R. *Prog. Inorg. Chem.* **1984**, *32*, 119.
(5) Auf der Heyde, T.; Bürgi, H.-B. *Inorg. Chem.* **1989**, *28*, 3961.
(6) Auf der Heyde, T.; Bürgi, H.-B. *Inorg. Chem.* **1989**, *28*, 3970.
(7) Auf der Heyde, T.; Bürgi, H.-B. *Inorg. Chem.* **1989**, *28*, 3982.
(8) Auf der Heyde, T. *Angew. Chem., Int. Ed. Engl.* **1994**, *33*, 823; *Angew. Chem.* **1994**, *106*, 871. For an overview see: *Structure Correlation;* Bürgi, H.-B., Dunitz, J. D., Eds.; VCH: Weinheim, 1993.
(9) CSD refcode NBCPTH, TACPTH. Wilson, R. D.; Koetzle, T. F.; Hart, D. W.; Kvick, Å.; Tipton, D. L.; Bau, R. *J. Am. Chem. Soc.* **1977**, *99*, 1775.
(10) Fachinetti, G.; Floriani, C.; Marchetti, F.; Merlino, S. *J. Chem. Soc., Chem. Commun.* **1976**, 522.
(11) Erker, G.; Wicher, J.; Engel, K.; Rosenfeld, F.; Dietrich, W.; Krüger, C. *J. Am. Chem. Soc.* **1980**, *102*, 6344.
(12) Yasude, H.; Tatsumi, K.; Nakamura, A. *Acc. Chem. Res.* **1985**, *18*, 120.
(13) Rüttger, D.; Erker, G. *Angew. Chem., Int. Ed. Engl.* **1997**, *36*, 812; *Angew. Chem.* **1997**, *109*, 840.
(14) Ballhausen, C. J.; Dahl, J. P. *Acta Chem. Scand.* **1961**, *15*, 1333.
(15) Brintzinger, H. H.; Bartell, L. S. *J. Am. Chem. Soc.* **1970**, *92*, 1105.
(16) Tatsumi, K.; Nakamura, A.; Hofmann, P.; Stauffert, P.; Hoffmann, R. *J. Am. Chem. Soc.* **1985**, *107*, 4440.
(17) Tatsumi, K.; Yasuda, H.; Nakamura, A. *Isr. J. Chem.* **1983**, *23*, 145.
(18) Gleiter, R.; Hyla-Kryspin, I.; Niu, S.; Erker, G. *Angew. Chem., Int. Ed. Engl.* **1993**, *32*, 754; *Angew. Chem.* **1993**, *105*, 753.
(19) Lauher, J. W.; Hoffmann, R. *J. Am. Chem. Soc.* **1976**, *98*, 1729.
(20) Brintzinger, H. H.; Fischer, D.; Mühlhaupt, R.; Rieger, B.; Waymouth, R. M. *Angew. Chem., Int. Ed. Engl.* **1995**, *34*, 1143; *Angew. Chem.* **1995**, *107*, 1255.
(21) For an overview see: *Ziegler Catalysts*; Fink, G., Mühlhaupt, R., Brintzinger, H. H., Eds.; Springer-Verlag: Berlin, 1995.
(22) Bochmann, M. *J. Chem. Soc., Dalton Trans.* **1996**, 255.
(23) Scollard, J. D.; McConville, D. H. *J. Am. Chem. Soc.* **1996**, *118*, 10008.
(24) Johnson, A. R.; Davies, W. M.; Cummins, C. C. *Organometallics* **1996**, *15*, 3825.
(25) Coles, M. P.; Dalby, C. I.; Gibson, V. C.; Clegg, W.; Elsegood, M. R. J. *J. Chem. Soc., Chem. Commun.* **1995**, 1709.
(26) Bazan, G. C.; Rodriguez, G.; Ashe, A. J.; Al-Ahmad, S.; Müller, C. *J. Am. Chem. Soc.* **1996**, *118*, 2291.
(27) Crowther, D. J.; Baenziger, N. C.; Jordan, R. F. *J. Am. Chem. Soc.* **1991**, *113*, 1455.
(28) Kreuder, C.; Jordan, R. F.; Zhang, H. *Organometallics* **1995**, *14*, 2993.

S0002-7863(97)02230-0 CCC: $14.00

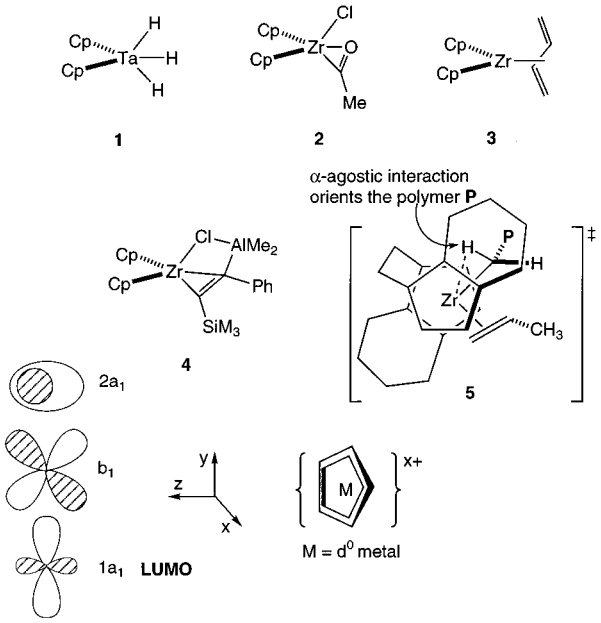

Figure 1. The three lowest lying unoccupied orbitals of the bent d^0 $\{MCp_2\}$ fragment dictate the coplanar arrangement of the $\{ML_3\}$ fragment in $[MCp_2L_3]$ complexes **1**−**4** and transition state **5**.

α-agostic interaction.[29−34] Brintzinger has proposed that this α-agostic interaction rigidifies the transition state structure of the C_2-symmetric catalyst during propylene insertion, thereby increasing the isotacticity of the resulting polypropylene. Specifically, the α-agostic interaction firmly orients the polymer chain into an open sector of the catalyst structure; this minimizes interaction between the alkyl substituent of the monomer and the ligand/polymer array during the insertion reaction.[35,36] Here again, **5** can be described neither as SPY-5 nor as TB-5.

In this context, the silyl-bridged amido−cyclopentadienyl ligand designed by Bercaw *et al.* also needs to be mentioned. It is used for the industrial production of polyethylene. An X-ray crystal structure of a five-coordinate hydride-bridged dimer, $[\{(\eta^5\text{-}C_5Me_4)Me_2Si(\eta^1\text{-}NCMe_3)\}(PMe_3)ScH]_2$ (**6**), reveals an EBT-5 geometry with an H−Sc−H angle of only 65.9° and an H−Sc−P angle of 68.8°.[37] Such compounds were found to polymerize α-olefins in a quasi-living manner. Structurally related zirconium complexes $[\{(\eta^5\text{-}C_5Me_4)Me_2Si(\eta^1\text{-}NCMe_3)\}\text{-}MeZr]^+$ have been patented as well.[38,39]

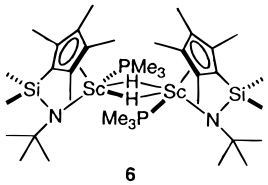

(29) Piers, W. E.; Bercaw, J. E. *J. Am. Chem. Soc.* **1990**, *112*, 9406.
(30) Grubbs, R. H.; Coates, G. W. *Acc. Chem. Res.* **1996**, *29*, 85.
(31) Fan, L.; Harrison, D.; Woo, T. K.; Ziegler, T. *Organometallics* **1995**, *14*, 2018.
(32) Woo, T. K.; Fan, L.; Ziegler, T. *Organometallics* **1994**, *13*, 2252.
(33) Woo, T. K.; Margl, P. M.; Lohrenz, J. C. W.; Blöchl, P. E.; Ziegler, T. *J. Am. Chem. Soc.* **1996**, *118*, 13021.
(34) Woo, T. K.; Fan, L.; Ziegler, T. *Organometallics* **1994**, *13*, 432.
(35) Krauledat, H.; Brintzinger, H. H. *Angew. Chem., Int. Ed. Engl.* **1990**, *29*, 1412; *Angew. Chem.* **1990**, *102*, 1459.
(36) Prosenc, M.-H.; Janiak, C.; Brintzinger, H. H. *Organometallics* **1992**, *11*, 4036.
(37) Shapiro, P. J.; Bunel, E.; Schaefer, W. P.; Bercaw, J. E. *Organometallics* **1990**, *9*, 867.
(38) Turner, H. W; Hlatky, G. G.; Canich, J. A. M. PTC Int. Appl. WO9319103; *Chem. Abstr.* **1994**, *120*, 271442.

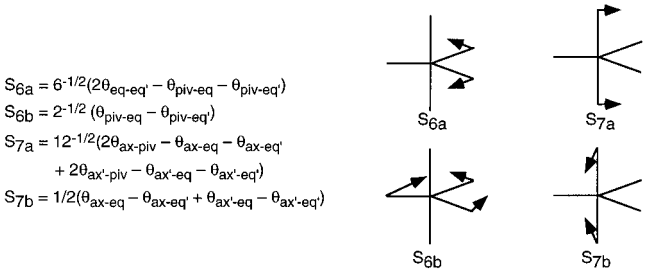

Figure 2. Sketch of the angular symmetry deformation coordinates with irreducible representation e′ for a trigonal bipyramidal molecule (point group symmetry D_{3h}).

In this study, we analyze the electronic requirements which may force five-coordinate d^0 complexes devoid of Cp ligands to adopt an EBT-5 geometry rather than the usual TB-5 or SPY-5 geometry. We also describe their relationship to the family of bent $[MCp_2L_3]$ complexes.

Results and Discussion

Theoretical Description of $[ML_5]^{x-}$ (L Is a *σ*-Donor). The geometries we are mainly concerned with, SPY-5 and EBT-5, can be considered as "small" angular distortions from an ideal TB-5 geometry. Such distortions are conveniently described in terms of seven linearly independent angular symmetry deformation coordinates.[40,41] Four of these, relevant to our study, are sketched in Figure 2. For the purpose of this paper, we refer to the ligands as L_{ax}, $L_{ax'}$, L_{eq}, $L_{eq'}$, and L_{piv}, where L_{piv} is the equatorial ligand not moving in S_{6a}. The SPY-5 geometry is achieved by deformation along S_{6a} and S_{7a}, the EBT-5 geometry by deformation primarily along $-S_{7a}$.

We begin our analysis with an extended Hückel (eH) description of the bonding of a trigonal bipyramidal five-coordinate d^0 complex containing pure *σ*-donors. A simplified molecular orbital diagram for a $[TiH_5]^-$ model is sketched in the middle of Figure 3.[3,42,43] The five ligand orbitals transform as $1a_1' + e' + a_2'' + 2a_1'$ ($2a_1'$ not shown) and interact with the $d_{x^2-y^2}$ (e′), d_{xz} (e′), d_{z^2} (a_1'), p_z (a_2''), and s (a_1') orbitals, respectively (abbreviated as $x^2 - y^2$, xz, z^2, z, etc., s not shown). The HOMO is a_2'' and is mostly ligand-centered. The *xy* and *yz* orbitals remain unperturbed and correspond to the LUMO (e″). It is the presence of these low-lying metal-centered orbitals, absent in main group compounds, which determines the ground state geometry of five-coordinate d^0 complexes. The second-order Jahn−Teller distortion[43] (2OJTD) occurs along the coordinates S_6 and S_7 of e′ symmetry which allows mixing of HOMOs and LUMOs ($\Gamma_{HOMO} \otimes \Gamma_{LUMO} = a_2'' \otimes e'' = e'$). As the LUMO is purely metal-based and the HOMO is mostly ligand-centered, electropositive *σ*-donors and/or electronegative metals should decrease the HOMO−LUMO gap, thereby accentuating the propensity for a 2OJTD.

A Walsh diagram for deformation along one of these e′ distortions, the one along $\pm S_{7a}$, is presented in Figure 3. By varying the $H_{piv}-Ti-H_{ax}$ angle α from 130° to 55°, we find two minima at 120° (E_{tot} = 0.00 eV) and 70° (E_{tot} = +0.22 eV) which correspond to the SPY-5 and EBT-5 geometries,

(39) Canich, J. A. M. U.S. Patent 5,026,798 to Exxon Chemical; *Chem. Abstr.* **1993**, *118*, 60284.
(40) Bürgi, H. B. *Inorg. Chem.* **1973**, *12*, 2321. Hoskins, L. C.; Lord, R. C. *J. Chem. Phys.* **1967**, *46*, 2402.
(41) In eH calculations, bond lengths cannot be optimized reliably, and their variations are therefore not considered.
(42) Albright, T. A.; Tang, H. *Angew. Chem., Int. Ed. Engl.* **1992**, *31*, 1462; *Angew. Chem.* **1992**, *104*, 1532. See also: Kang, S. K.; Tang, H.; Albright, T. A. *J. Am. Chem. Soc.* **1993**, *115*, 1971.
(43) Albright, T. A.; Burdett, J. K.; Whangbo, M.-H. *Orbital Interactions in Chemistry*; John Wiley: New York, 1985.

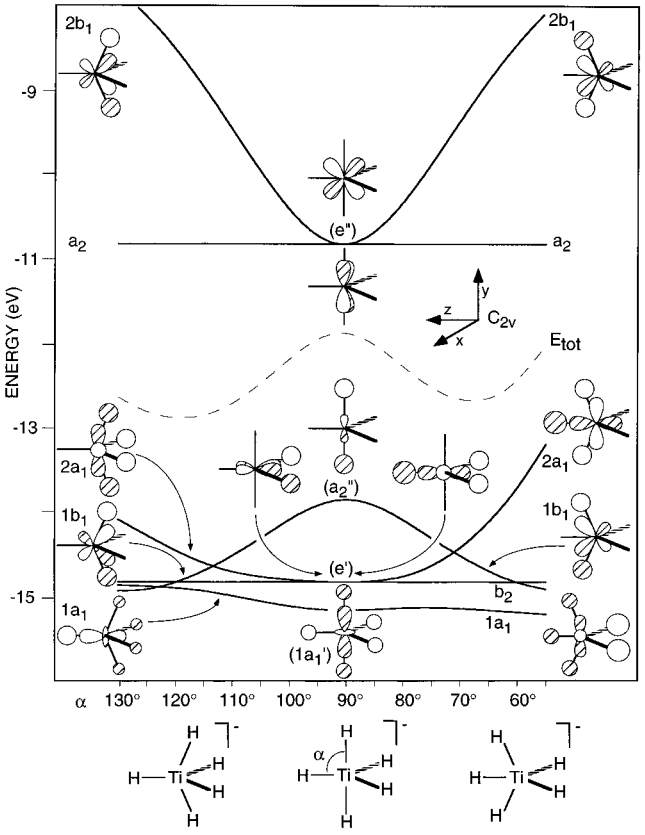

Figure 3. Walsh diagram for the SPY-5 → TB-5 → EBT-5 interconversion of $[TiH_5]^-$. (Dotted line, E_{tot}; labels in parentheses correspond to D_{3h} irreducible representations).

respectively. TB-5 ($\alpha = 90°$, $E_{tot} = +1.00$ eV) is a transition state in this diagram. The total energy follows mostly the fate of the a_2'' orbital in D_{3h} symmetry which becomes b_1 in C_{2v}. The SPY-5 vs EBT-5 preference can be traced back to a difference in ligand−ligand interactions associated with the $2a_1$ orbital: artificially setting the $L_{ax}-L_{eq}$ and $L_{ax}-L_{piv}$ overlaps to zero reduces the energetic advantage of SPY-5 over EBT-5 to only 0.05 eV. The total energy is fairly insensitive to the $L_{eq}-Ti-L_{eq'}$ angle γ. For all three geometries EBT-5, TB-5, and SPY-5, $\gamma = 120°$ affords the lowest energy.

As mentioned above, the 2OJTD for d^0 systems follows a doubly degenerate e′ coordinate. So far, we have analyzed a bending of the $L_{ax}-M-L_{ax'}$ fragment toward L_{piv}. This bending could also take place in the direction of L_{eq} or $L_{eq'}$ or in any direction in between. We measure this direction by the precession angle β about the y axis measured relative to the vertical mirror plane of EBT-5 and illustrated in **7**.[44]

The whole e′ distortion pathway was probed by independently varying $0° \le \beta \le 360°$ and $55° \le \alpha \le 90°$. The resulting potential energy surface (PES) is presented in Figure 4a, with ordinate $\cos\alpha \sin\beta$ and abscissa $\cos\alpha \cos\beta$. These coordinates represent the projection of $M-L_{ax}$ unit vectors onto the equatorial plane $ML_{eq}L_{eq'}L_{piv}$. This PES shows the expected Mexican hat features with three minima and three saddle points corresponding to the SPY-5 ($\alpha = 60°$, $\beta = 60°$, 180°, and 300°) and EBT-5 ($\alpha = 70°$, $\beta = 0°$, 120°, and 240°) geometries, respectively. EBT-5, which appears as a minimum in the Walsh diagram $E = f(\alpha)$ (Figure 3), is in fact a saddle point on the

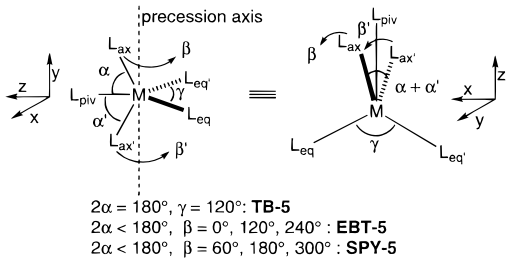

7

two-dimensional surface ($E = f(\alpha,\beta)$) and lies well below the maximum representing TB-5.

In order to obtain more accurate results, density functional calculations were performed on the model $[TiH_5]^-$ (see the Appendix for computational details). The Ti−H bond lengths were first optimized with the local density approximation (Vosko−Wilk−Nusair, LDA) along the totally symmetric a_1' breathing mode in D_{3h} symmetry. The bond lengths yielding the minimum energy were then used to generate the PES ($E = f(\alpha,\beta)$) at the same level of approximation (LDA), as well as at the nonlocal (Becke−Perdew, BP) level. The resulting DFT-BP PES is depicted in Figure 4b. Finally, the geometry of the extrema (TB-5 and SPY-5) was fully optimized at the LDA and BP levels. The relevant structural features are summarized in Figure 5. The PES obtained from eH and DFT (LDA and BP) calculations display similar overall features. In both cases, a Mexican hat-like PES is computed with a high-lying TB-5 transition state, low-lying ETB-5 saddle points, and SPY-5 minima.

It thus appears that, irrespective of the level of theory (eH, DFT-LDA, DFT-BP), the predicted ground state geometry of d^0 $[ML_5]$ complexes with five σ-donating ligands is SPY-5. Further, the complexes may well show fluxional behavior which does not involve TB-5 but EBT-5 transition states.

A Cambridge Structural Database (CSD) search revealed a single homoleptic compound containing five pure σ-donors around a d^0 metal: $[Ta(CH_2(4\text{-}MeC_6H_4))_5]$.[45] Its SPY-5 structure ($2\alpha = 138.1°$, $\beta = 177.2°$, and $\gamma = 137.0°$) is depicted in **8**. Recently, the structure of $[TaMe_5]$ was determined by gas phase electron diffraction. In contrast to its main group counterpart $[SbMe_5]$, the d^0 complex has a SPY-5 geometry.[42,46]

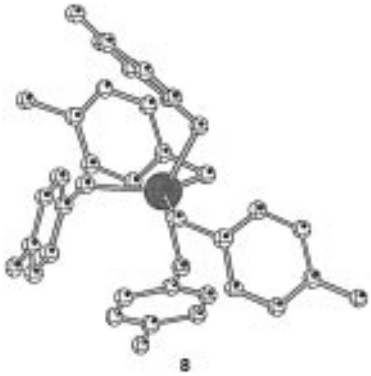

8

Theoretical Description of $[MD_2L_3]^{x-}$ (D Is a π-donor). Coordinatively saturated $[MCp_2L_3]$ complexes differ from the above models; they contain two cylindrical π-donating cyclopentadienyls in equatorial positions. As will be shown below,

(44) α, α' and β, β' are the polar coordinates of unit $M-L_{ax}$ vectors. They are related to S_{7a} and S_{7b} by $2\alpha \propto (S_{7a}^2 + S_{7b}^2)^{1/2}$ and $tg\beta = S_{7b}/S_{7a}$. Since variations in the $L_{eq}-M-L_{eq'}$ angle γ affect calculated eH energies only little, this angle is not varied in the calculation of potential energy surfaces described below, but is occasionally mentionned for experimentally determined structures.

(45) CSD refcode HEDCUW. Piersol, C. J.; Profilet, R. D.; Fanwick, P. E.; Rothwell, I. P. *Polyhedron* **1993**, *12*, 1779.

(46) Pulham, C.; Haaland, A.; Hammel, A.; Rypdal, K.; Verne, H. P.; Volden, H. V. *Angew. Chem., Int. Ed. Engl.* **1992**, *31*, 1464; *Angew. Chem.* **1992**, *104*, 1534.

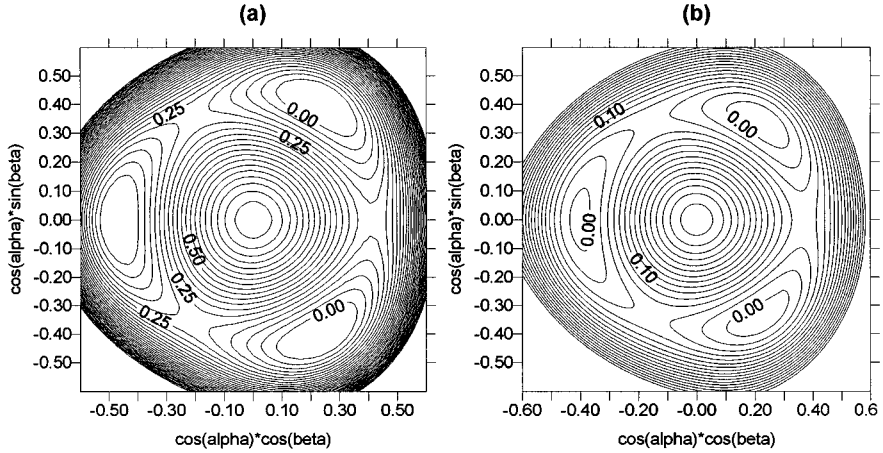

Figure 4. Potential energy surface $E = f(\alpha,\beta)$ for the SPY-5 → TB-5 → EBT-5 interconversion of $[TiH_5]^-$: (a) eH level of theory, (b) DFT-BP (the coordinates, abscissa = cos α cos β, ordinate = cos α sin β, correspond to the position of an M−L_{ax} unit vector projected onto the *yz*-plane containing the $ML_{eq}L_{eq'}L_{piv}$ fragment, equienergy contours in electronvolts).

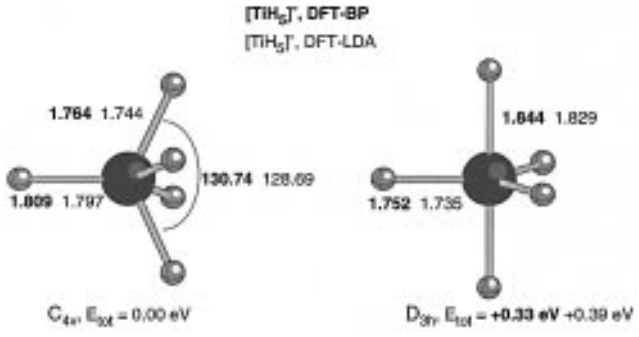

Figure 5. DFT-optimized geometry of $[TiH_5]^-$.

the presence of π-donors D affects the ground state geometry of $[MD_2L_3]^{x-}$ complexes, eventually favoring EBT-5 over SPY-5.

Introducing different ligands into TB-5 complexes, e.g., weak and strong σ-donors or single- and double-faced π-donors, raises the problem of site and orientation preference. For TB-5 geometries, the strongest σ-donors bind preferentially in the equatorial plane, relegating the electronegative and hence weaker, donors to axial positions.[3,43] As σ-effects dominate over π-effects, electronegative weak cylindrical π-donors are predicted to bind in a diaxial geometry. This has been verified computationally for $[Ta(OPh)_2H_3]$. Related structures determined experimentally will be discussed in the section on structure correlation. Conversely, strong cylindrical π-donors adopt a bisequatorial geometry as computed for the hypothetical bisalkylidyne $[Ti(CH)_2H_3]^{5-}$. Trigonal bipyramidal complexes containing two single-faced π-donors can assume nine different configurations, differing in the position of the π-donors (axial/equatorial) and the orientation of their filled π-orbital (parallel, ||, or perpendicular, ⊥, to the equatorial plane). The three most stable diastereomers of the bis-alkylidene $[Ti(CH_2)_2H_3]^{3-}$ are depicted in **9a**−**c**. Interestingly, **9d** is the least stable of all isomers.

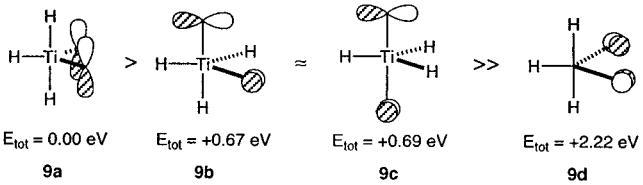

The π-orientation preference of **9a** over **9d** can be traced to the fact that, for **9d**, the M−C π-interactions compete with σ-bonding in the equatorial plane. For the $p^+_{||}$ fragment molecular orbital (FMO) in **10a**, this yields increased overlap with the metal-centered FMOs which are polarized away from H_{piv} to minimize the H_{piv}−M antibonding interaction. However, due to its M−H σ-antibonding character, this metal-centered FMO has a poor energy match with the $p^+_{||}$ FMO. The stabilization energy, as predicted by perturbation theory, is thus small. The other combination, $p^-_{||}$ (b_2) in **10b**, is essentially nonbonding, because the corresponding metal *xz* orbital is mostly involved in M−C σ-bonding. Both $p^+_{\perp}$ (b_1) and $p^-_{\perp}$ (a_2) interact efficiently with pure *yz* and *xy* orbitals as seen in **11b** and **11a**, respectively. Despite slightly smaller overlaps, the good energy match between the FMO's determines the preferred orientation of the π-donors.

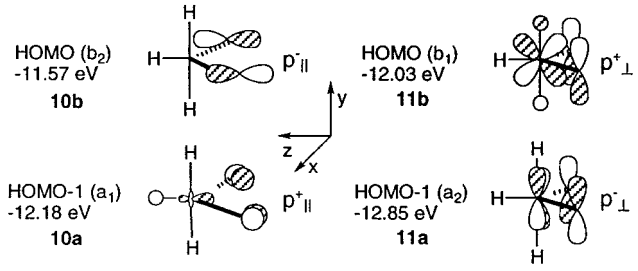

Having delineated some factors important in determining the site and orientation preference of π-donors in TB-5 $[MD_2H_3]^{x-}$ complexes, we focus on the 2OJTD for $[MD_2H_3]^{x-}$. We tackle the problem by analyzing $[Ti(NH_2)_2H_3]^-$ which contains two single-faced π-donors. The amides are positioned in the equatorial plane with their occupied p_y orbital perpendicular to it. A Walsh diagram $E = f(\alpha)$, 130° > α > 55°, for the distortion SPY-5 → TB-5 → EBT-5 is presented in Figure 6. As for $[TiH_5]^-$ (Figure 3), we find two minima, but this time, EBT-5 (α = 70°, γ = 120°, E_{tot} = 0.00 eV) lies well below SPY-5 (α = 110°, γ = 120°, E_{tot} = +0.91 eV). A slightly distorted TB-5 (α = 95°, γ = 120°, E_{tot} = +1.00 eV) is the transition state. Remember that, in the distorted C_{2v} form of the pure σ-donor complex $[TiH_5]^-$, the orbitals of the b_1 irreducible representation determine to a large extent the shape of the Mexican hat PES. The in-phase combination of the p_y orbitals of $[Ti(NH_2)_2H_3]^-$, abbreviated $Np_{\perp}^+$, also has b_1 irreducible representation; it therefore interacts with the b_1 molecular orbitals built from the ligand σ-orbitals and affects the appearance of the PES. To trace down the reversal of geometric preference from SPY-5 to EBT-5, a simplified

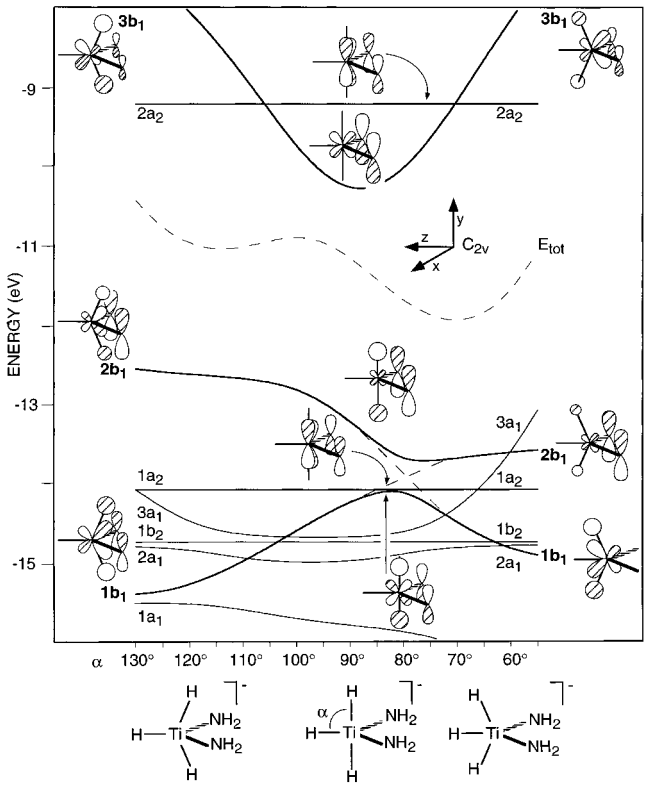

Figure 6. Walsh diagram for the SPY-5 → TB-5 → EBT-5 interconversion of $[Ti(NH_2)_2H_3]^-$. Only the MOs containing $Np_\perp$ contributions are sketched. All other MOs are very similar to those of Figure 3 (dotted line, E_{tot}).

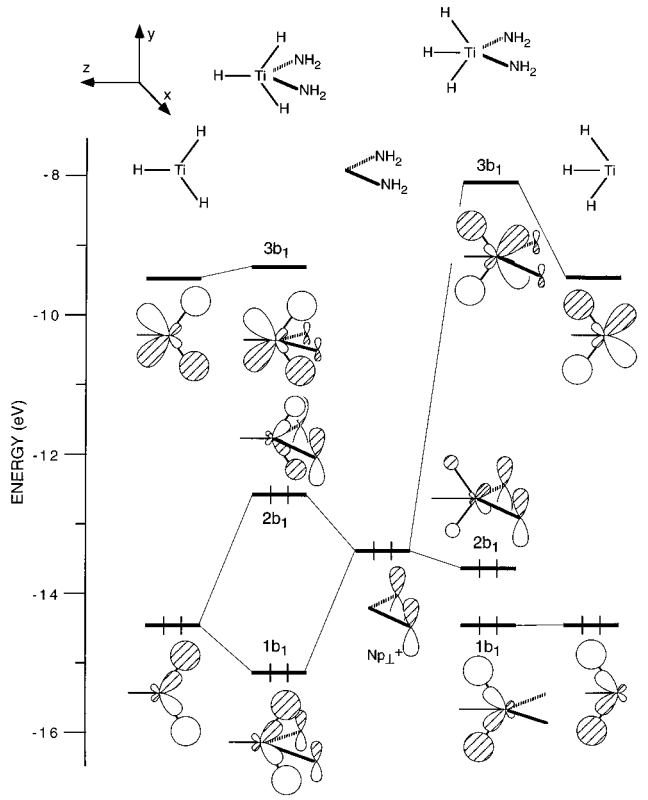

Figure 7. Simplified interaction diagram of $\{TiH_3\}^+$ and $\{(NH_2)_2\}^{2-}$ fragment molecular orbitals in the EBT-5 (right) and SPY-5 (left) geometries of $[Ti(NH_2)_2H_3]^-$ (Only b_1 irreducible representations shown).

interaction diagram containing the three relevant fragment orbitals of the b_1 irreducible representation is sketched in Figure 7.

For each geometry, we build $[Ti(NH_2)_2H_3]^-$ from two fragments: $\{TiH_3\}^+$ and $\{(NH_2)_2\}^{2-}$. On the $\{TiH_3\}^+$ fragment, the lower orbital is Ti−H bonding, while the upper one is Ti−H nonbonding. Hybridization of the metal *yz* and *y* orbitals maximizes Ti−H bonding ($1b_1$ MO) and minimizes antibonding ($2b_1$ MO), respectively. The even higher lying Ti−H antibonding combination is not shown. As the minima are computed for $\alpha = 70°$ and 110° for EBT-5 and SPY-5, respectively, the Ti−H overlaps are identical for both $\{TiH_3\}^+$ fragments. Therefore, all three interacting FMOs, namely, Ti−H bonding, Ti−H nonbonding, and $Np_\perp^+$, have identical energies for both geometries: −14.5, −9.4, and −13.4 eV, respectively.

In the case of SPY-5, the Ti−H bonding FMO has a good energy match and overlap with the $Np_\perp^+$ FMO. This leads to an efficient interaction, yielding a Ti−N bonding and a Ti−N antibonding MO, both filled MOs. The Ti−H nonbonding FMO hardly interacts with the $Np_\perp^+$ FMO as it is polarized away from the Ti−N vector (Figure 7, left).

The situation is reversed in EBT-5. The Ti−H bonding FMO is polarized away from the Ti−N vector. Despite a good energy match with the $Np_\perp^+$ orbital, the overlap is small and this orbital remains mostly Ti−N nonbonding. The $Np_\perp^+$ orbital has a strong overlap with the Ti−H nonbonding FMO in the EBT-5 geometry, but the poor energy match prevents efficient interaction between the two FMOs. As a consequence, the two filled MOs of the b_1 irreducible representation in EBT-5 $[Ti(NH_2)H_3]^-$ are mostly Ti−N nonbonding (Figure 7, right).

Overall, the $2b_1$ antibonding combination in SPY-5 is more destabilized than its $1b_1$ bonding counterpart is stabilized, and the EBT-5 situation is favored energetically as both $1b_1$ and $2b_1$ are essentially Ti−N nonbonding. The reverse tendency seen for $[TiH_5]^-$, namely, a preference of SPY-5 due to the a_1 orbitals, is overcompensated by the effects of the b_1 orbitals in $[Ti(NH_2)_2H_3]^-$.

In going from $[TiH_5]^-$ to $[Ti(NH_2)_2H_3]^-$, the symmetry of the TB-5 reference geometry is reduced from D_{3h} to C_{2v}. This is reflected in the two-dimensional PES $E = f(\alpha,\beta)$: only two minima are found (Figure 8a). The more stable one at $\alpha = 70°$ corresponds to EBT-5; the very shallow, higher lying minimum corresponds to SPY-5. They are connected by a transition state at $\alpha = 97°$.[47] The deformation takes place in the plane bisecting the $\{Ti(NH_2)_2\}$ fragment, either away from or toward the two NH_2 ligands. Note that the distortions away from or toward a single NH_2 group no longer lead to an extremum as was found for $[TiH_5]^-$ (Figure 4). Nevertheless, the remnants of the Mexican hat PES of Figure 4 are still found in Figure 8a. The more stable minimum is shallower in the direction that corresponds to a change of the precession angle β than in the direction which changes only α. This feature will be important in discussing experimental structural data.

DF calculations were also performed on the model $[Ti(NH_2)_2H_3]^-$. The $Ti-H_{piv} = Ti-H_{ax}$ and $Ti-N_{eq}$ bond lengths were first optimized with LDA in a TB-5 geometry (all angles as well as N−H bond lengths frozen). The resulting geometry was then used to generate the PES ($E = f(\alpha,\beta)$) at the same level of approximation. The computed DFT-LDA PES is depicted in Figure 8b. The geometry of the minimum (EBT-5) was then fully optimized at the LDA and BP levels. The relevant structural features are summarized in Figure 9.

In contrast to the eH PES obtained for $[Ti(NH_2)_2H_3]^-$, no extrema are found for TB-5 and SPY-5 geometries, but the

(47) Similar calculations were repeated with the parameters of all metals from groups 4−7. The shallow SPY-5 minimum was obtained at $\alpha = 110°$ only with the Ti parameters. For all other calculations (both at the DFT and eH levels of theory), the minimum at $\alpha \approx 110°$ becomes a flat region on the PES $E = f(\alpha,\beta)$.

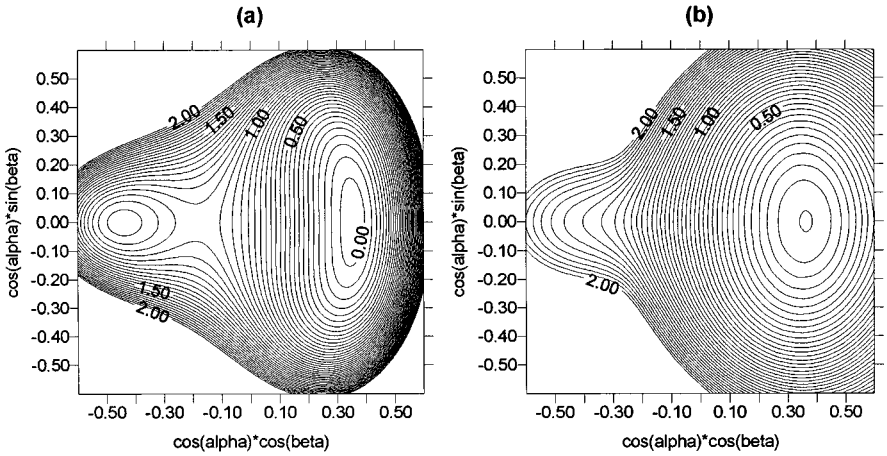

Figure 8. Potential energy surface $E = f(\alpha,\beta)$ for the SPY-5 → TB-5 → EBT-5 interconversion of $[Ti(NH_2)_2H_3]^-$: (a) eH level of theory, (b) DFT-LDA (for a definition of coordinates, see Figure 4).

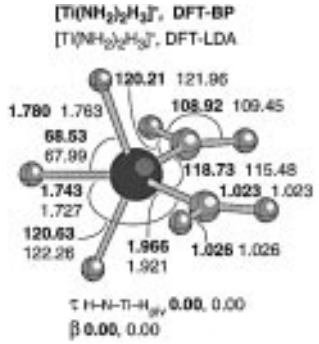

Figure 9. DFT-optimized geometry of $[Ti(NH_2)_2H_3]^-$.

overall shape of the EBT-5 minimum is maintained. The LDA and BP ground state geometries closely resemble that computed with eH for $[Ti(NH_2)_2H_3]^-$.[47]

Introduction of two double-faced π-donors in the equatorial plane of TB-5 was probed with the model $[Ti(NH)_2H_3]^{3-}$. Neither $Np_{||}^+$ **10a** nor $Np_{||}^-$ **10b** contribute significantly to the EBT-5 preference, which is dictated by the fragment orbital $Np_\perp^+$ **11b**. However, as the Ti−N distance decreases on going from an amido (Ti−N 1.94 Å) to an imido group (Ti−N 1.76 Å), the Ti−N overlap increases, further favoring EBT-5 over SPY-5. Within the range of α and β investigated here ($0° \le \beta \le 360°$ and $55° \le \alpha \le 90°$), this model yields a single minimum for the EBT-5 geometry. Here again, deformations of the β angle do not destabilize the system significantly.

The model $[Ti(NH)_2H_3]^{3-}$ is directly comparable to $[TiCp_2H_3]$. The role in metal−ligand binding of the "sp" lone pair of NH is analogous to that of the nodeless π-orbital of Cp; similarly the role of the two p-orbitals of NH is comparable to that of the two degenerate π-orbitals of Cp with a single nodal plane. For comparison, we computed an $E = f(\alpha,\beta)$ PES for the metallocene model $[TiCp_2H_3]^-$. The overall feature resembles Figure 8. However, the EBT-5 absolute minimum ($E_{tot} = 0.00$ eV, $\alpha = 65°$, $\beta = 0°$, $\gamma = 136°$) is very deep, and small distortions both in the α and β directions are costly in energy. In its TB-5 geometry ($E_{tot} = +1.95$ eV), the HOMO−LUMO gap of $[TiCp_2H_3]^-$ is only 2.20 eV (compared to 3.03 eV for $[Ti(NH_2)_2H_3]^-$). As a result, the HOMO−LUMO mixing along the e′ 2OJTD coordinate is more efficient and accounts for the acute α in the EBT-5 ground state. The distortion along the β coordinate is disfavored purely on steric grounds: at $\alpha = 65°$ and $\beta = 30°$, the shortest $H_{ax}-H_{Cp}$ and $H_{ax}-C_{Cp}$ contacts are 2.05 and 2.02 Å, respectively. By artificially setting the $H_{ax}-H_{Cp}$ and $H_{ax}-C_{Cp}$ overlaps to zero, the shallow minimum observed for $[Ti(NH_2)_2H_3]^-$ in EBT-5 is restored and the β-precession about the *y* axis is soft.

It remains to investigate the effects of replacing the σ-donating ligands L in our model $[M(NH)_2L_3]^{x+}$ by π-donors which are weak compared to NH. If one considers the imides as 6-electron donors, a d^0 complex would be coordinatively saturated with three pure σ-donors L completing the coordination sphere. If L is a potential π-donor, it competes for π-interactions with the imides. The resulting ground state geometry will be determined by a delicate balance between π-donation and steric interactions. Let us illustrate this point with a few examples.

The presence of a third, albeit weaker, π-donor in the equatorial plane of $[Ti(NH)_2H_2Cl_{piv}]^{3-}$ prevents efficient *yz*/*y* hybridization and reduces the driving force for distortion toward EBT-5 relative to $[Ti(NH)_2H_3]^{3-}$. As a consequence, $[Ti(NH)_2H_2Cl_{piv}]^{3-}$ is calculated to adopt an EBT-5 geometry with α approaching 90°. The presence of cyclopentadienyls, which are both bulky and strongly π-donating, forces the $[TiCp_2H_2Cl_{piv}]^{3-}$ complex back into an EBT-5 geometry ($\alpha = 77°$); see **12**. Adding two chlorides in the axial positions in

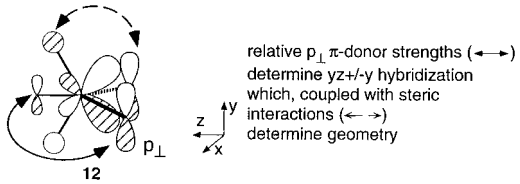

$[Ti(NH)_2Cl_2H_{piv}]^{3-}$ yields an EBT-5 with $\alpha = 80°$, and $\beta = 0°$. In this case, the efficiency of the 2OJTD away from the TB-5 geometry is hampered by the large HOMO−LUMO gap caused by the presence of electronegative axial chlorides. For $[Ti(NH)_2Cl_3]^{3-}$, where three chlorides complete the coordination sphere, we compute a nearly perfect TB-5 equilibrium structure. As the TB-5 geometry is sterically highly unfavorable when two cyclopentadienyls are present, $[TiCp_2Cl_3]^{3-}$ adopts a EBT-5 geometry with $\alpha = 80°$ and $\beta = 0°$.

In summary, the geometry adopted by five-coordinate d^0 -$[MD_2L_3]$ complexes with strong, single- or double-faced π-donors D as well as that adopted by $[MCp_2L_3]$ complexes is the result of the same 2OJTD along a *reversed-Berry coordinate*. From our model calculations, it appears that *all* d^0 systems containing only two strong single-faced π-donors in the equatorial plane with their filled p-orbital perpendicular to this plane ($p_\perp$) should display an EBT-5 geometry. In the following section, we test this model with structural data retrieved from the Cambridge Structural Database (CSD) (June 1996 version).

Table 1. Complexes Containing Two Strong π-Donors in the Equatorial Plane[a]

entry	M	L_{eq}	$L_{eq'}$	L_{pivot}	L_{ax}	$L_{ax'}$	2α	β_{mean}	δ	γ	ref
1	Ta	$CHBu^t$	$CHBu^t$	Mes	PMe_3	PMe_3	166.3	4.8	6.9	109.0	55
2	Ta	$NSiR_3$	$NSiR_3$	Py	Me	Py	151.9	4.7	2.0	115.3	52
3	Mo	O	O	Mes	Mes	CH_2PR_3	151.0	16.2	4.5	113.5	56
4	Re	O	O	Np	Np	Np	149.7[b]	93.0	−12.5[c]	117.3	53
5	Re	O	O	SAr	Np	Np	149.5[b]	1.2	−0.2[c]	117.8	57
6	Re	NAr	NAr	Me	Np	Np	147.7	0.8	0.5	130.8	58
7	W	O	NEt_2	Np	Np	Np	145.8	20.0	11.2	118.8	54

[a] Py = pyridine, Np = neopentyl, Ar = substituted phenyl group. [b] $|\alpha - \alpha'| > 5°$. [c] β and δ move in the same direction, see **13**.

Structure Correlation. After defining and retrieving the structures of interest, we map the available structures in the two-dimensional configuration space spanned by α and β. As observed structures tend to concentrate in low-lying regions of the potential energy surface,[8] we compare structural scatterplots with the results of eH calculations for analogous model compounds. The points in such plots which are far from the computed minima will be discussed individually in an attempt to trace down their particularity.

(a) Fragment Definition. We searched all d^0 five-coordinate complexes. The metals considered were Sc(III), Y(III), Ti(IV), Zr(IV), Hf(IV), V(V), Nb(V), Ta(V), Cr(VI), Mo(VI), W(VI), Mn(VII), Tc(VII), and Re(VII). Only those compounds containing two of the following strong π-donors were retrieved: alkylidyne, alkylidene, nitrido, phosphoraniminato (1−), hydrazido (2−), imido, amido, oxo, and alkoxo ligands.[48] To ensure that the geometry is not biased by ligand constraints, all polynuclear complexes were excluded, as well as those containing chelating or η^n-arene ligands ($n > 1$).

To our surprise, this search yielded no more than five five-coordinated d^0 complexes containing *only* two strong π-donors. We thus relaxed our definition to include complexes containing two strong π-donors and up to three weaker π-donors: halides and N-bonded aromatic heterocycles, yielding a total of 29 complexes. In the presence of good π-donors such as dianionic or trianionic C, N, and O ligands, alkoxides can be considered comparatively weaker and were included as well to afford a total of 36 complexes: one V(V), four Nb(V), eight Ta(V), six Mo(VI), five W(VI), and twelve Re(VII) complexes. These are listed in Tables 1−4.

For comparison, all $[MCp_2L_3]$-like complexes were retrieved from the CSD database. These are listed in Table 5 and Figure 13. Again here, only mononuclear complexes and those containing no chelates are considered, yielding six Zr(IV), five Ta(V), and four Nb(V) complexes. Of these sixteen hits, the last three contain hydride atoms for which no positional coordinates are available.

(b) Ligand Labeling and Distortion Mapping. In order to unambiguously determine the relevant distortion angles, a consistent ligand labeling scheme is required. Since the complexes can be viewed as distorted TB-5, one large (<180°), three medium (∼120°), and six small (∼90°) interligand angles are expected. After computing all 10 interligand angles for each complex, the largest angle was assigned as the $L_{ax}-M-L_{ax'}$ angle. The remaining three ligands were taken to define the equatorial plane.

In those cases where two large angles (∼150°) were computed, thus suggesting an SPY-5 coordination, the equatorial plane was defined in terms of the two strongest π-donor ligands D and D′ and the remaining equatorial ligand L_{piv}. With the exception of five bisaxial alkoxide complexes listed in Table 2, this simple procedure allows us to consistently label all complexes. Having assigned the equatorial *xz* plane, containing L_{piv}, L_{ax}, and $L_{ax'}$, the metal was placed at the origin. In the spirit of the ideal C_{2v}-symmetric EBT-5 geometry, the *yz* plane was defined to be perpendicular to the *xz* plane and to bisect the D−M−D′ angle. On the basis of this coordinate system, all relevant angles where calculated.[49] The ligands L_{ax} and $L_{ax'}$ are not always identical, and thus α and α' or β and β' are not always the same; only the sum $\alpha + \alpha' = 2\alpha$ and β_{mean} are reported in Tables 1−5. Note that, for $2\alpha = 180°$, β is not defined. For 2α close to 180°, β values are meaningless. Since D_{eq} is not always identical to $D_{eq'}$, the ligand L_{piv} does not necessarily lie in the bisecting plane; its deviation from this plane is measured by δ; see **13**.[50] As in the theoretical section, we map the distortion angles α and β, by looking at the projection of unit $M-L_{ax}$ vectors in the *xz* plane containing the ligands D_{eq}, $D_{eq'}$ and L_{piv}. The necessary relationships are $x = \cos\alpha \sin\beta$ and $z = \cos\alpha \cos\beta$.

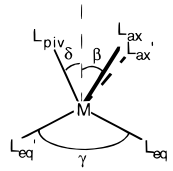

13

We have shown in the theoretical section that the geometry of five-coordinate d^0 complexes $[MD_2L_3]^{x-}$, incorporating two strong π-donors D, depends critically on the ancillary ligands L. The 36 compounds listed in Tables 1−5 are categorized according to the donor properties of L. The corresponding Figures 10−13 map the experimental structures together with an eH equienergy contour which lies 0.1 eV above the energy minimum calculated for an appropriate model compound. The horizontal dotted line corresponds to a bending of the axial ligands away from the π-donor ligands, i.e., to EBT-5 geometries. The diagonal dotted lines correspond to bending of the axial ligands toward one or the other π-donor, corresponding to a different type of EBT-5 geometry. Analogously, the horizontal solid line describes a bending of the axial ligands toward the π-donors, i.e., SPY-5 geometries. The diagonal solid lines imply bending of the axial ligands away from one of the two π-donors, leading to different SPY-5 configurations. This geometry is expected for complexes bearing only one strong

(48) Nugent, W. A.; Mayer, J. M. *Metal-Ligand Multiple Bonds*; John Wiley & Sons: New York, 1988.

(49) In the experimental structures, M is not necessarily coplanar with the equatorial plane defined by L_{eq}, $L_{eq'}$, and L_{piv}. However, this does not affect the definitions of α and β. The angles α and α' are the complement to 90° of the angles between the $M-L_{ax}$ and $M-L_{ax'}$ vectors and the *y* axis. The angles β and β' are the angles between the *z* axis and the projections of the $M-L_{ax}$ and $M-L_{ax'}$ vectors onto the *xz* plane.

(50) In the theoretical analysis described above, L_{ax} and $L_{ax'}$ were identical and rotated by the same amount and in opposite directions about the *x* axis, thus defining the α-distortion. Similarly, the β-precession of both L_{ax} and $L_{ax'}$ about the *y* axis was synchronous. In reality, however, L_{ax} need not be the same as $L_{ax'}$ and neither of these distortions need be synchronous. The entries in Tables 1−5 which display marked asynchronous distortions are superscripted accordingly.

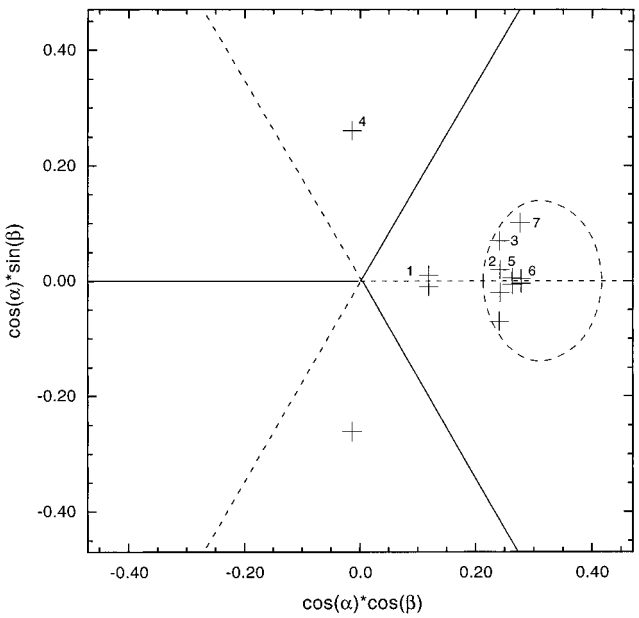

Figure 10. Mapping of $[MD_2L_3]^{x-}$ structures (D = strong π-donor, L = pure σ-donor). The dotted circular line represents the 0.1 eV eH isoenergy contour computed for $[Ta(NH)_2H_3]^{2-}$ (for a definition of coordinates, see Figure 4).

equatorial π-donor.[51] All lines intersect at the origin which corresponds to TB-5. Compounds incorporating two chemically equivalent strong π-donors are displayed twice, i.e., at $\pm\cos\alpha \sin\beta$. Compounds $[MDD'L_3]^{x-}$ with two different π-donors D and D′ are displayed only with positive ordinates.

(c) Structural Scatterplots. Complexes bearing only two equatorial π-donors are listed in Table 1. In addition, we included one complex containing two pyridine ligands which are notably weak π-donors (entry 2).[52] One complex with L_{piv} = thiophenolate was included as well, as the sulfur π-orbital is oriented in the equatorial plane and thus does not compete with the oxo $p_\perp$ orbitals responsible for the 2OJTD (entry 5). The observed structural data are displayed in Figure 10, along with the eH isoenergy contour at 0.1 eV for the model $[Ta(NH)_2H_3]^{2-}$. In most compounds of this class, the axial substituents bent away from the π-donors and toward the pivot ($2\alpha < 180°$ and $\beta < 30°$). Five of the seven compounds are within the minimum energy region calculated for the model complex $[Ta(NH)_2H_3]^{2-}$. Exceptions are entries 1 and 4.

Entry 1, $[Ta(CHBu^t)_2Mes(PMe_3)_2]$, follows the reversed-Berry coordinate. Both carbenes are oriented properly to favor an efficient 2OJTD. Relatively short H−H contacts (2.19 Å) between the axial PMe_3 and the pivotal mesitylene prevent further bending of L_{ax} toward L_{piv}. Entry 4, $[ReO_2(Np)_3]$, **14**, is very unusual.[53] It reveals a strong interaction between a methylene hydrogen from each axial neopentyl group and one of the two equatorial oxygens (H···O distances 2.08 and 2.26 Å). This leads to a significant lengthening of the corresponding Re═O bond (1.81 Å vs 1.66 Å), accompanied by a decrease in π-donation from O to Re.

Systems incorporating one strong and one weaker π-donor can be expected to adopt geometries intermediate between EBT-5, encountered with two strong π-donors, and SPY-5, a geometry prevalent with five-coordinate compounds bearing a single π-donor.[48,51] Such an intermediate geometry is observed not only for $[ReO_2(Np)_3]$ (**14**) but also for $[WO(NEt_2)Np_3]$ (**15**) (entry 7).[54] In both cases, the axial ligands precess toward the weaker π-donor, the longest, most distant oxo and the amide groups, respectively.

Table 2. Complexes Containing Two π-Donors as Axial Ligands[a]

entry	M	L_{eq}	$L_{eq'}$	L_{pivot}	L_{ax}	$L_{ax'}$	2α	β_{mean}	δ	γ	ref
8	Ta	Np	Np	Np	OAr	OAr	178.3	4.9	1.0	127.3	59
9	Nb	Bz′	Bz′	Bz′	OAr	OAr	174.8	129.1	0.1	121.2	60
10	Ta	Bz′	Bz′	Bz′	OAr	OAr	174.5	134.0[b]	0.4	122.0	60
11	Ta	Bz	Bz	Bz	OAr	OAr	165.6	160.0	0.1	127.8	61
12	Ta	Me	Me	Me	OAr	OAr	163.9	2.1	0.7	105.2	62

[a] Bz′ = substituted benzyl. [b] $|\beta - \beta'| > 15°$.

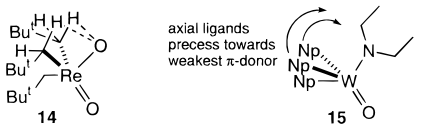

Overall, the distortion away from TB-5 is less pronounced than for bent metallocene complexes $[MCp_2L_3]$ (Table 5), but does follow the same reversed-Berry pathway.

When very bulky aromatic alkoxides and three alkyl ligands are present, the two electronegative weakly π-donating ligands occupy axial positions; i.e., the σ-site preference dominates π-effects (Table 2). This arrangement also minimizes the steric interactions and yields complexes approaching TB-5, in agreement with theoretical results. The α, β projections of all five compounds nearly coincide with the 0.1 eV isosurface of the model $[Ta(OPh)_2H_3]$ (mapping not shown).

Complexes bearing two strong and one weaker equatorial π-donors are listed in Table 3. The general picture is as expected. Fluoride which is generally considered the strongest π-donor among the halide ions, efficiently competes with the oxo ligands for π-interactions; see **12**. It is thus not surprising that $[VO_2F(Pz')_2]$ adopts a nearly perfect TB-5 geometry (Pz′ = substituted pyrazole, entry 13). Despite the presence of a pivotal chloride in $[Nb(NAr)_2Cl_{piv}(PMe_3)_2]$,[63] the 2OJTD is efficient: 2α is compressed to 148.4°, perhaps due to the presence of strong axial σ-donors (entry 17). In comparison, 2α expands to 161.5° on going to the poorer σ-donor pyridine in $[Ta(NAr)_2Cl_{ax}Py_2]$ (entry 16).[64]

(51) DuBois, D. L.; Hoffmann, R. *New J. Chem.* **1977**, *1*, 479.
(52) CSD refcode PAVFEX. Schaller, C. P.; Wolczanski, P. T. *Inorg. Chem.* **1993**, *32*, 131.
(53) CSD refcode FUWLAK. Cai, S.; Hoffman, D. M.; Wierda, D. A. *J. Chem. Soc., Chem. Commun.* **1988**, 313.
(54) CSD refcode VUMGOZ. Le Ny, J. P.; Youinou, M.-T.; Osborn, J. A. *Organometallics* **1992**, *11*, 2413.
(55) CSD refcode NPYTAP10. Churchill, M. R.; Youngs, W. J. *Inorg. Chem.* **1979**, *18*, 1930.
(56) CSD refcode DULFEV. Laï, R.; Le Bot, S.; Baldy, A.; Pierrot, M.; Arzoumanian, H. *J. Chem. Soc., Chem. Commun.* **1986**, 1208.
(57) CSD refcode JAWBEO. Cai, S.; Hoffman, D. M.; Wierda, D. A. *Inorg. Chem.* **1989**, *28*, 3784.
(58) CSD refcode JILCUC. Cook, M. R.; Herrmann, W. A.; Kiprof, P.; Takacs, J. *J. Chem. Soc., Dalton Trans.* **1991**, 797.
(59) CSD refcode DERGEM. LaPointe, R. E.; Wolczanski, P. T.; Duyne, G. D. V. *Organometallics* **1985**, *4*, 1810.
(60) CSD refcode JIHWOM, JIHWIG. Chesnut, R. W.; Jacob, G. G.; Yu, J. S.; Fanwick, P. E.; Rothwell, I. P. *Organometallics* **1991**, *10*, 321.
(61) CSD refcode FOVCOI. Chamberlain, L. R.; Rothwell, I. P.; Folting, K.; Huffman, J. C. *J. Chem. Soc., Dalton Trans.* **1987**, 155.
(62) CSD refcode BUNJUP10. Chamberlain, L. R.; Rothwell, I. P.; Huffman, J. C. *J. Am. Chem. Soc.* **1986**, *108*, 1502.
(63) CSD refcode ZAZDEJ. Bott, S. G.; Hoffman, D. M.; Rangarajan, S. P. *Inorg. Chem.* **1995**, *34*, 4305.
(64) CSD refcode VIDVEJ. Chao, Y.-W.; Wexler, P. A.; Wigley, D. E. *Inorg. Chem.* **1990**, *29*, 4592.
(65) CSD refcode YOGJAF. Mohan, M.; Bond, M. R.; Otieno, T.; Carrano, C. J. *Inorg. Chem.* **1995**, *34*, 1233.
(66) CSD refcode VUGTUM. Dilworth, J. R.; Jobanputra, P.; Parrott, S. J.; Thompson, R. M.; Povey, D. C.; Zubieta, J. A. *Polyhedron* **1992**, *11*, 147.
(67) CSD refcode BIFRAG. Chatt, J.; Crichton, B. A. L.; Dilworth, J. R.; Dahlstrom, P.; Gutkoska, R.; Zubieta, J. *Inorg. Chem.* **1982**, *21*, 2383.

Table 3. Complexes Containing Three π-Donors in the Equatorial Plane[a]

entry	M	L_{eq}	$L_{eq'}$	L_{pivot}	L_{ax}	$L_{ax'}$	2α	β_{mean}	δ	γ	ref
13	V	O	O	F	Pz′	Pz′	177.6	118.2[b]	3.1	114.9	65
14	Re	O	NNPhMe	Cl	PPh_3	PPh_3	172.1	24.8	6.4	110.7	66
15	Mo	$NNMe_2$	$NNMe_2$	Cl	PPh_3	PPh_3	170.6	32.9	7.3	112.2	67
16	Ta	NAr	NAr	Cl	Py	Py	161.5	28.3[b]	3.3	113.2	64
17	Nb	NAr	NAr	Cl	PMe_3	PMe_3	148.4	33.8	5.6	114.2	63

[a] Pz′ = substituted pyrazole. [b] $|\beta - \beta'| > 15°$.

Table 4. Complexes Containing Axial and Equatorial π-Donors

entry	M	L_{eq}	$L_{eq'}$	L_{pivot}	L_{ax}	$L_{ax'}$	2α	β_{mean}	δ	γ	ref
18	Re	CBu^t	$CHBu^t$	THF	OR_F	OR_F	128.6	8.6	40.1	102.5	68
19	Mo	$NNAr_2$	$NNAr_2$	Cl	Cl	PPh_3	166.6	15.7[b]	0.3	115.3	69
20	Mo	O	O	$OSiPh_3$	$OSiPh_3$	PPh_3	166.5	3.0	2.0	110.0	70
21	W	NAr	CHR	OR_F	OR_F	NR_3	163.9	1.3	9.5	100.7	71
22	W	NAr	CHR	OR_F	OR_F	$P(OMe)_3$	163.7	20.2[b]	18.6	98.8	72
23	W	$CHBu^t$	O	Cl	Cl	PEt_3	163.4	11.1[b]	9.8	106.8	73
24	Mo	$CHBu^t$	NAr	OR_F	OR_F	PMe_3	162.0	3.5	10.8	110.7	71
25	Re	N	$NNArPh_2$	Cl	Cl	PPh_3	161.7[a]	32.7[b]	13.8	107.5	74
26	W	$NSiMe_3$	$NSiMe_3$	Cl	Cl	PPh_2Me	161.2	13.5	−1.5[c]	110.0	75
27	Re	NBu^t	NBu^t	Cl	Cl	Ph	157.7	10.0	9.1	110.1	76
28	Re	NBu^t	NBu^t	Cl	Cl	Ar	146.4[a]	32.2	25.6	108.0	77
29	Re	NNR_2	NNR_2	Cl	Cl	Cl	170.8	8.0	0.3	119.7	78
30	Re	NNR_2	NNR_2	$OSiMe_3$	Cl	Cl	170.6	15.4	0.4	114.8	78
31	Re	NBu^t	NBu^t	Cl	Cl	Cl	165.4	9.0	3.2	110.7	76
32	Nb	$NPPh_3$	$NPPh_3$	Cl	Cl	Cl	161.5	27.1	11.0	109.0	79
33	Re	NAr	$CHBu^t$	OAr	OAr	OAr	160.7	12.6[b]	37.3	100.0	80
34	Mo	N	$NPPh_3$	Cl	Cl	Cl	160.0	25.2	18.7	106.1	81
35	Nb	OAr	OAr	Cl	Cl	Cl	153.9	46.0	26.8	103.8	82
36	Ta	OAr	OAr	Cl	Cl	Cl	143.8	44.1	27.9	104.2	83

[a] $|\alpha - \alpha'| > 5°$. [b] $|\beta - \beta'| > 15°$. [c] β and δ move in the same direction; see **13**.

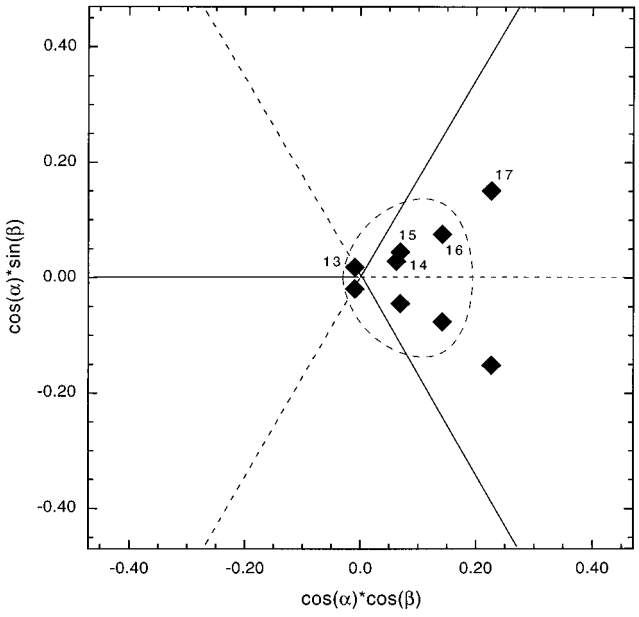

Figure 11. Mapping of $[MD_2BL_2]^{x-}$ structures (D = equatorial strong π-donor, B = pivot π-donor, L = pure σ-donor). The dotted circular line represents the 0.1 eV eH isoenergy contour computed for $[Ta(NH)_2Cl_{piv}H_2]^{2-}$ (for a definition of coordinates, see Figure 4).

Next, we consider a complex incorporating strong equatorial as well as weaker axial π-donors, Table 4 and Figure 12. The geometry of $[Re(CBu^t)(CHBu^t)\{OCCH_3(CF_3)_2\}_2$ (THF)] (**16**), entry 18,[68] is unique: the pivotal site is occupied by a very loosely-bound THF (Re−O 2.40 Å), which has precessed, however, by an unusually large angle δ of ∼40° toward the weakest carbon π-donor. The resulting structure resembles a face-capped tetrahedron more than EBT-5.

Complexes incorporating weak π-donors L_{piv} and L_{ax} nicely follow the reversed-Berry pathway. As discussed above, those with two different π-donors, i.e., electronic asymmetry, bend toward the weaker π-donor, yielding distorted EBT-5 structures (entries 19−27). Bisimido complex $[Re(NAr)_2Cl_2Ar]$ (entry 28, $\beta = 32°$, $\delta = 26°$) displays a nearly perfect SPY-5 geometry. The strong π-donors are electronically asymmetric as one imido is linear, Re−N−C = 176.4°, and one is bent, Re−N−C =

(68) CSD refcode PAGMIT. Toreki, R.; Schrock, R. R.; Davis, W. M. *J. Am. Chem. Soc.* **1992**, *114*, 3367.
(69) CSD refcode YELXUI. Bustos, C.; Manzur, C.; Carrillo, D.; Robert, F.; Gouzerh, A. *Inorg. Chem.* **1994**, *33*, 4937.
(70) CSD refcode PERGAU. Huang, M.; DeKock, C. W. *Inorg. Chem.* **1993**, *32*, 2287.
(71) CSD refcode VIZMAZ, VIZMEW. Schrock, R. R.; Crowe, W. E.; Bazan, G. C.; DiMare, M.; O'Regan, M. B.; Schofield, M. H. *Organometallics* **1991**, *10*, 1832.
(72) CSD refcode YAVTUK. Johnson, L. K.; Grubbs, R. H.; Ziller, J. W. *J. Am. Chem. Soc.* **1993**, *115*, 8130.
(73) CSD refcode CLNPOW10. Churchill, M. R.; Missert, J. R.; Youngs, W. J. *Inorg. Chem.* **1981**, *20*, 3388.
(74) CSD refcode VAXGOR. Dilworth, J. R.; Jobanputra, P.; Miller, J. R.; Parrott, S. J.; Chen, Q.; Zubieta, J. *Polyhedron* **1993**, *12*, 513.
(75) CSD refcode KEGTIZ. Lichtenhan, J. D.; Critchlow, S. C.; Doherty, N. M. *Inorg. Chem.* **1990**, *29*, 439.
(76) CSD refcode JIBSUI, JIBSOC. Danopoulos, A. A.; Longley, C. J.; Wilkinson, G.; Hussain, B.; Hursthouse, M. B. *Polyhedron* **1989**, *8*, 2657.
(77) CSD refcode KATTAA. Longley, C. J.; Savage, P. D.; Wilkinson, G.; Hussain, B.; Hursthouse, M. B. *Polyhedron* **1988**, *7*, 1079.
(78) CSD refcode WEPBOI, WEBPIC. Danopoulos, A. A.; Wilkinson, G.; Williams, D. J. *J. Chem. Soc., Dalton Trans.* **1994**, 907.
(79) CSD refcode JUHNAB. Weller, F.; Nusshär, D.; Dehnicke, K. *Z. Anorg. Allg. Chem.* **1992**, *615*, 7.
(80) CSD refcode VIZTED. Schofield, M. H.; Schrock, R. R.; Park, L. Y. *Organometallics* **1991**, *10*, 1844.
(81) CSD refcode JUWHEO. Nusshär, D.; Weller, F.; Dehnicke, K. *Z. Anorg. Allg. Chem.* **1993**, *619*, 507.
(82) CSD refcode ZEQTEU. Lockwood, M. A.; Potyen, M. C.; Steffey, B. D.; Fanwick, P. E.; Rothwell, I. P. *Polyhedron* **1995**, *14*, 3293.
(83) CSD refcode COLVII. Chamberlain, L. R.; Rothwell, I. P.; Huffman, J. C. *Inorg. Chem.* **1984**, *23*, 2575.

Table 5. $[Cp_2ML_3]$-like Complexes[a]

entry	M	L_{eq}	$L_{eq'}$	L_{piv}	L_{ax}	L_{ax}	2α	β_{mean}	δ	γ	ref
37	Zr	Cp	Cp	OTs	H_2O	H_2O	148.0[b]	0.5	1.5	135.7	85
38	Zr	Cp	Cp	H_2O	H_2O	H_2O	145.2	6.3	0.3	134.9	86
39	Zr	Cp	Cp	THF	OTf	OTf	140.9	2.0	1.9	132.9	87
40	Ta	Cp	Cp	$SnCl_2Me$	H	H	131.5	4.4	3.0	148.2	88
41	Ta	Cp	Cp	H	H	H	125.8	0.1	0.5	147.0	9
42	Nb	Cp	Cp	H	H	H	125.7	6.2	0.3	149.2	9
43	Zr	Cp	Cp	H	PMe_3	PMe_3	119.6	0.4	4.2	133.4	89
44	Nb	CpTMS	CpTMS	$SiHPh_2$	H	H	115.4	11.6[c]	6.3	136.2	90
45	Zr	Cp	Cp	H	$SiMe_3$	PPh_3	112.7	1.0	2.9	141.1	91
46	Nb	Cp	Cp	$AsEt_2$	H	H	112.1[b]	5.5	0.6	145.3	92
47	Nb	Cp	Cp	H	$SiMe_2Cl$	$SiMe_2Cl$	104.2[b]	1.2	1.8	143.8	93
48	Ta	Cp	Cp	PPh_2	H	H	102.1[b]	22.3[c]	−2.7[d]	143.1	94
49	Ta	Cp	Cp	H	$SiHMe_2$	$SiHMe_2$	109.9			144.3	95
50	Ta	Cp	Cp	$SiMe_2Ph$	H	H	*e*			144.7	96
51	Zr	C_5Me_5	C_5Me_5	H	H	H	*e*			144.1	97

[a] Ts = tosylate, Tf = triflate, TMS = trimethylsilyl. [b] $|\alpha - \alpha'| > 5°$. [c] $|\beta - \beta'| > 15°$. [d] β and δ move in the same direction; see **13**. [e] H atoms not localized.

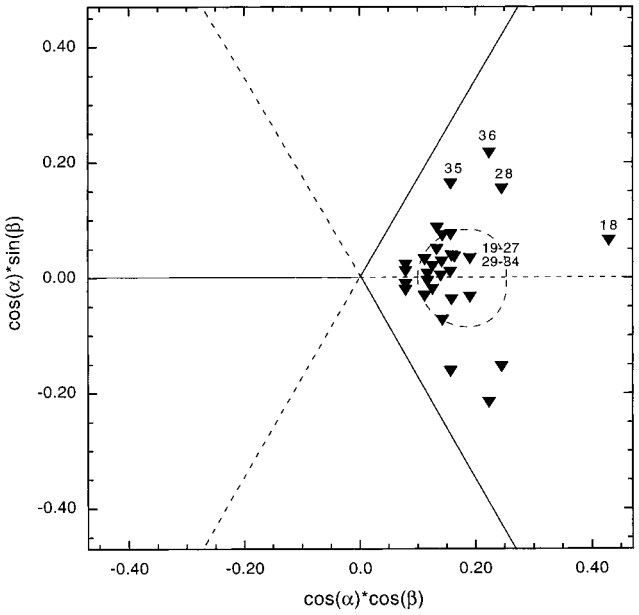

Figure 12. Mapping of $[MD_2Z_3]^{x-}$ structures (D = equatorial strong π-donor, Z = σ-donor or weak π-donor). The dotted circular line represents the 0.1 eV eH isoenergy contour computed for $[Ta(NH)_2H_{piv}Cl_2]^{2-}$ (for a definition of coordinates, see Figure 4).

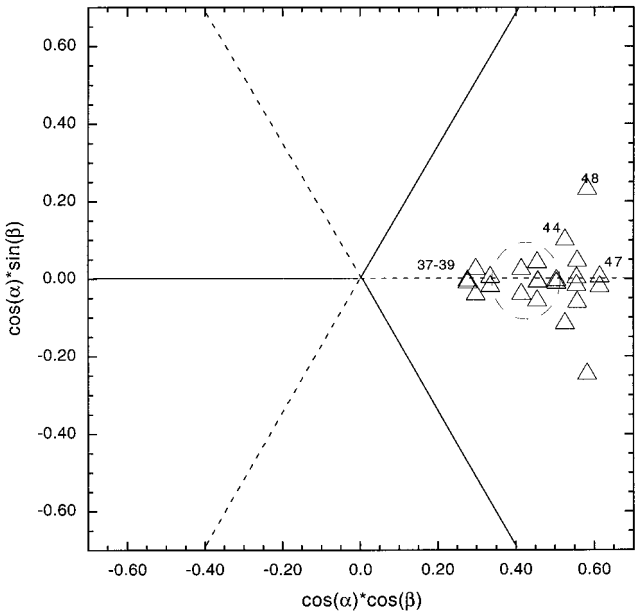

Figure 13. Mapping of $[MCp_2L_3]^{x-}$ structures. The dotted circular line represents the 0.1 eV eH computed isoenergy contour for $[TaCp_2H_3]$ (for a definition of coordinates, see Figure 4).

150.5°. The axial ligands bend *away* from the stronger of the two, analogous to the situation in **14**, **15**, and **17**.

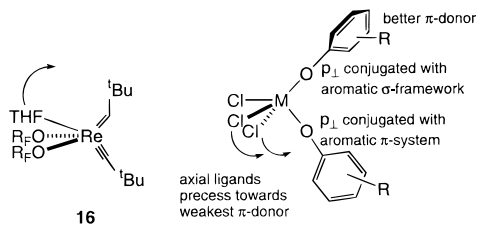

Complexes with three weak π-donors adopt very similar geometries (entries 29−36), with the exception of both bisalkoxo complexes which are best described as SPY-5. Although both alkoxo ligands are linear, their π-orbitals are electronically asymmetric as one shows $p_\perp$ conjugated with the aromatic π-system (weaker π-donor), while the other is hyperconjugated with the ligand σ-framework. The axial ligands precess toward the weakest alkoxo ligand, as illustrated in **17**. In other words, they bend away from the better of the two donors ($\cos\alpha \cos\beta > 0$) and are never found between them ($\cos\alpha \cos\beta < 0$). This implies that the electronically driven distortion discussed in the theoretical part is operative, but leads to an ideal EBT-5 only if L_{eq} and $L_{eq'}$ are structurally, conformationally, and electronically identical.

Finally, we note that an inequivalence of L_{eq} and $L_{eq'}$ also affects the position of L_{piv}: if L_{ax} and $L_{ax'}$ deviate from the bisector plane in one direction, L_{piv} tends to deviate from this plane in the opposite direction and by about half as much. Such a distortion, characterized by the angle δ, corresponding to a distortion along S_{6b}, opens up one of the $L_{piv}-L_{eq}$ angles, eventually leading to a SPY-5 geometry with both basal angles ($L_{ax}-M-L_{ax'}$; $L_{piv}-M-L_{eq}$) $\gg 120°$.

As discussed in the theoretical section, the 2OJTD is more efficient for cyclopentadienyl ligands than for other strong π-donors. For $[MCp_2L_3]$ complexes, the 2α angles fall in the range 148.0−102.1°. It is interesting to note that the complexes which are least bent are those with the most electronegative L_{ax}: electropositive axial donors favor the 2OJTD. This is nicely reflected with compounds containing axial silanes (Table 5, entries 45, 47, and 49) which all display very acute $L_{ax}-M-L_{ax'}$ angles, despite significant steric interactions with L_{piv}. Except for two compounds (entries 44 and 48), the β angle is

very small. Entries 46 and 48 contain a pivot ligand capable of π-donation. However, the pyramidalization at As and P, respectively, clearly points toward a localized lone pair and thus no significant π-bonding.[84]

Conclusion and Outlook

We have shown that five-coordinate d^0 complexes tend to show an EBT-5 geometry when two strong π-donors are incorporated into equatorial positions with their π-orbitals perpendicular to the equatorial plane of the distorted TB-5. This geometry can be considered as the result of a 2OJTD along a reversed-Berry pathway. We find that the 2OJTD is maximal in the absence of further π-donors L in the coordination sphere of $[MD_2L_3]^{x-}$. The compounds are analogous structurally and electronically to the bent metallocenes $[MCp_2L_3]^{x-}$. However, these latter display a larger degree of 2OJTD. On one hand, the cyclopentadienyl ligand is an ideal π-donor. Not only does this yield a small HOMO−LUMO gap in the TB-5 geometry, it also prevents other potential π-donors in the coordination sphere of $[MCp_2L_3]^{x-}$ from interacting efficiently via a π-interaction. On the other hand, steric interactions between Cp and L_{ax}, $L_{ax'}$, and L_{piv} keep β and δ small and thus L_{ax}, $L_{ax'}$, and L_{piv} coplanar.

Our theoretical model was tested, and the results from a structure-correlation analysis of all d^0 five-coordinate complexes incorporating two strong π-donors lead to the same conclusion: the presence of two strong but different π-donors, i.e., electronic asymmetry, favors structures intermediate between SPY-5 and EBT-5. In the spirit of Muetterties and Guggenberger's mapping of the Berry pathway,[2] the d^0 complexes containing two π-donors can be arranged in a sequence that maps a reversed-Berry pathway (Figure 14).[98]

The three lowest lying empty orbitals of $\{Cp_2Ti\}^{2+}$ and $\{Ti(NH_2)_2\}^{2+}$ are compared in Figure 15.[99] These orbitals have similar composition and the same energetic ordering, and thus both fragments can be coined isolobal.[25,71,100−102] We believe, however, that these fragments are unique to systems incorporating a transition metal. To illustrate our point, let us mention the nucleophilic attack on four-coordinate tetrahedral systems. In main group chemistry, such a reaction occurs on the face of the tetrahedron, eventually leading to TB-5; see **18**. Formally, four-coordinate metallocenes and their relatives undergo nucleophilic attack on an *edge* of the tetrahedron, to yield EBT-5 geometries, which is the landmark of such systems; see **19**.[16]

One major advantage of Cp ligands over other strong π-donors, often triply bonded ligand atoms, is the ease of incorporating sterically demanding groups capable of efficiently interacting with coordinated substrates and promoting catalytic transformations at the metal template to proceed in a stereospecific manner. The isolobal relationship presented in this work could form a basis for the synthesis of EBT-5 complexes with other sterically demanding π-donors. Bercaw's mixed Cp/amide complex **6** is a first step in this direction. A further step is the titanium-based chelating bisamide system, $[Ti(RN(CH_2)_3NR)Me_2]$, R = substituted arene, recently reported by McConville and Scollard. In the presence of $B(C_6F_5)_3$, this

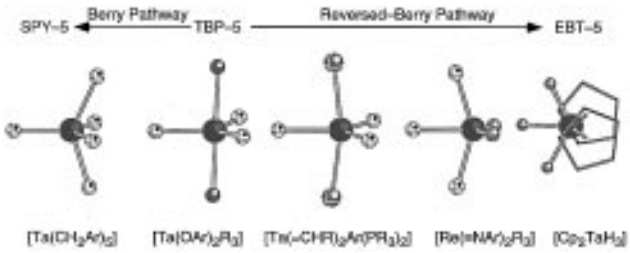

Figure 14. Mapping of the reversed-Berry pathway with five-coordinate d^0 complexes incorporating two π-donors and three σ-donors.

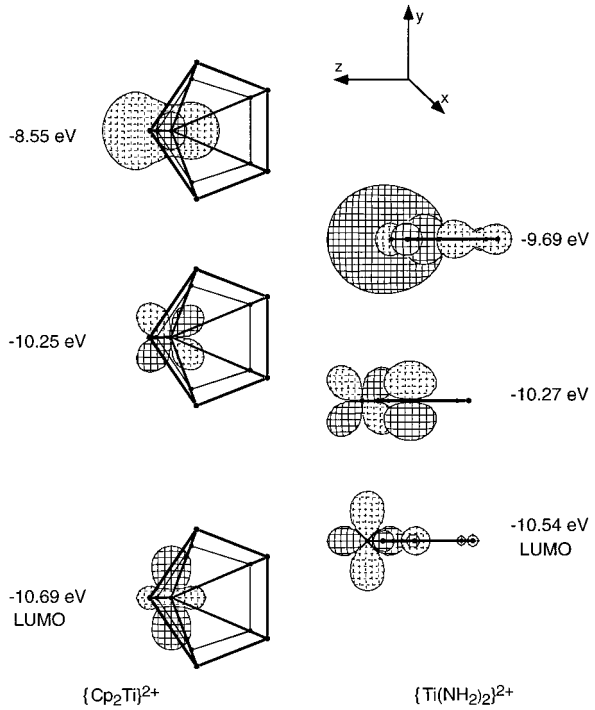

Figure 15. The three lowest lying empty orbitals of $\{TiCp_2\}^{2+}$ (left, Cp contributions not shown) and $\{Ti(NH_2)_2\}^{2+}$ (right), generated with the CACAO program.

(84) Baker, R. T.; Whitney, J. F.; Wreford, S. S. *Organometallics* **1983**, *2*, 1049.
(85) CSD refcode DOKCAH. Lasser, W.; Thewalt, U. *J. Organomet. Chem.* **1986**, *302*, 201.
(86) CSD refcode CAXBOS. Thewalt, U.; Lasser, W. *J. Organomet. Chem.* **1984**, *276*, 341.
(87) CSD refcode CAXBIM. Thewalt, U.; Lasser, W. *Z. Naturforsch. B* **1983**, *38*, 1501.
(88) CSD refcode FEZCUI. Arkhireeva, T. M.; Bulychev, B. M.; Protsky, A. N.; Soloveichik, G. L.; Bel'sky, V. K. *J. Organomet. Chem.* **1986**, *317*, 33.
(89) CSD refcode FIPTED. Jordan, R. F.; Bajgur, C. S.; Dasher, W. E.; Rheingold, A. L. *Organometallics* **1987**, *6*, 1041.
(90) CSD refcode YOTNAV. Antinolo, A.; Carrillo, F.; Fajardo, M.; Otero, A.; Lanfranchi, M.; Pellinghelli, M. A. *Organometallics* **1995**, *14*, 1518.
(91) CSD refcode KONREK. Kreutzer, K. A.; Fisher, R. A.; Davis, W. M.; Spaltenstein, E.; Buchwald, S. L. *Organometallics* **1991**, *10*, 4031.
(92) CSD refcode YUBNOY. Nikonov, G. I.; Lorberth, J.; Harms, K.; Lemenovskii, D. A. *Inorg. Chem.* **1995**, *34*, 2461.
(93) CSD refcode ZEYVAA. Nikonov, G. I.; Kuzmina, L. G.; Lemenovskii, D. A.; Kotov, V. V. *J. Am. Chem. Soc.* **1995**, *117*, 10133.
(94) CSD refcode ZEQFEG. Nikonov, G. I.; Kuzmina, L. G.; Mountford, P.; Lemenovskii, D. A. *Organometallics* **1995**, *14*, 3588.
(95) CSD refcode KOKVOV. Jian, Q.; Carroll, P. J.; Berry, D. H. *Organometallics* **1991**, *10*, 3648.
(96) CSD refcode DADWIO. Curtis, M. D.; Bell, L. G.; Butler, W. M. *Organometallics* **1985**, *4*, 701.
(97) CSD refcode ZIWSED. Fermin, M. C.; Stephan, D. W. *J. Am. Chem. Soc.* **1995**, *117*, 12645.
(98) The $L_{eq}-M-L_{eq'}$ angles γ reported in Tables 1-5 have not been explicitly discussed. As the γ_{mean} for the compounds listed in Tables 1, 3, and 4 is 110.8°, i.e., <120°, the 2OJTD leading to EBT-5 proceeds along both $-S_{7a}$ and $-S_{6a}$ as expected for a reversed-Berry deformation.
(99) Brintzinger and Bartell[15] arrived at the orbitals of Figure 15 along a different route. They considered the 2OJTD of a linear, sandwich-type $[TiCp_2]$ geometry.
(100) Elian, M.; Chen, M. M. L.; Mingos, D. M. P.; Hoffmann, R. *Inorg. Chem.* **1976**, *15*, 1148.
(101) Hoffmann, R. *Angew. Chem., Int. Ed. Engl.* **1982**, *21*, 711; *Angew. Chem.* **1982**, *94*, 724.
(102) Dyer, P. W.; Gibson, V. C.; Howard, J. A. K.; Whittle, B.; Wilson, C. *J. Chem. Soc., Chem. Commun.* **1992**, 1666.

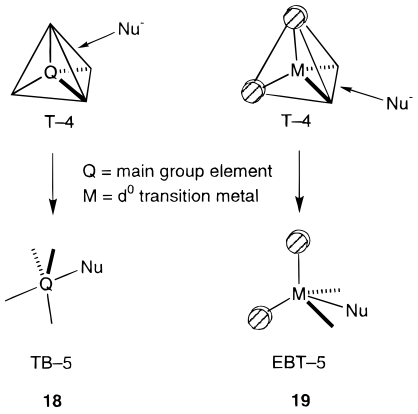

18 **19**

complex polymerizes propene in a living manner.[23,103] The chelate ring enforces proper orientation of the N_π-orbitals, and the amide offers an opportunity to incorporate steric bulk, which could well yield promising stereospecific catalytic systems.

Appendix

All eH calculations[104−106] were performed with the CACAO program.[107] All the parameters used were taken from previous calculations.[19,108] In this paper, we describe the results obtained with the Ti (theoretical part) and Ta parameters (structure correlation). Very similar results for the most relevant cases were computed with other metal parameters including Zr, V, Cr, Mo, and Re. The following bond lengths[109] were used for the eH calculations: Ti−H 1.7 Å, Ti−Cl 2.30 Å, Ti−$Cp_{centroid}$ 2.06 Å, C−C 1.40 Å, C−H 1.05 Å, Ti−NH_2 1.94 Å, Ti−NH 1.76 Å, N−H 1.02 Å, Ta−H 1.77 Å, Ta−Cl 2.40 Å, Ta−NH 1.76 Å, Ta−OAr 1.5 Å, O−C_{Ar} 1.32 Å.

Density Functional Calculations. The Hartree−Fock−Slater combination of Atomic orbitals (HFS-LCAO) as implemented in the Amsterdam density functional (ADF) program developed by Baerends *et al.* was used.[110−113] The potential energy surface calculations were performed using the Vosko−Wilk−Nusair (VWN, LDA) exchange-correlation potential.[114] The extrema ($[TiH_5]^-$, TB-5 and SPY-5; $[Ti(NH_2)_2H_3]^-$, ETB-5) were then fully optimized with VWN augmented with Becke's approximation for the exchange and Perdew's for the correlation (DFT-BP).[115−118] For $[TiH_5]^-$, a PES was generated with DFT-BP, yielding a picture very similar to that obtained with the VWN. Therefore, for $[Ti(NH_2)_2H_3]^-$, only the DFT-LDA PES was computed. The ADF atomic orbitals were described using an uncontracted triple-ζ Slater-type orbital basis set on Ti and augmented by single polarization functions both on C and H. The 1s shell of carbon and 1s2s2p3s3p3d shells of titanium were assigned to the core and treated using the frozen core approximation.[111] A set of auxiliary s, p, d, f, and g functions, centered on all nuclei, was used to fit electron density together with both Coulomb and exchange potentials in each SCF cycle.[119]

Acknowledgment. We dedicate this work to Professor Roald Hoffmann on the occasion of his 60th birthday. T.R.W. thanks Dr. Dario Veghini for stimulating discussions as well as Professor A. Ludi for his hospitality. We thank Dr. Jürg Hauser for help with the Cambridge Structural Database. Financial support comes from the Swiss National Science Foundation and from *Stiftung für Stipendien auf dem Gebiete der Chemie* (Award of a Werner Fellowship to T.R.W., 1994−1999).

JA972230S

(103) Tinkler, S.; Deeth, R. J.; Duncalf, D. J.; McCamley, A. *Chem. Commun.* **1996**, 2623.
(104) Hoffmann, R.; Lipscomb, W. N. *J. Chem. Phys.* **1962**, *36*, 2179, 3489.
(105) Hoffmann, R. *J. Chem Phys.* **1963**, *39*, 1397.
(106) Ammeter, J. H.; Bürgi, H.-B.; Thibeault, J. C.; Hoffmann, R. *J. Am. Chem. Soc.* **1978**, *100*, 3686.
(107) Mealli, C.; Proserpio, D. M. *J. Chem. Educ.* **1990**, *67*, 399.
(108) Hoffman, D. M.; Hoffmann, R.; Fiesel, C. R. *J. Am. Chem. Soc.* **1982**, *104*, 3858.
(109) Orpen, A. G.; Brammer, L.; Allen, F. H.; Kennard, O.; Watson, D. G.; Taylor, R. *J. Chem. Soc., Dalton Trans.* **1989**, S1.
(110) Baerends, E. J.; Ellis, D. E.; Ros, P. *Chem. Phys.* **1971**, *2*, 41.
(111) Ravenek, W. *Algorithms and Applications on Vector and Parallel Computers*; Elsevier: Amsterdam, 1987.
(112) Te Velde, G.; Baerends, E. J. *J. Comput. Phys.* **1992**, *99*, 84.
(113) Boerrigter, P. M.; Te Velde, G.; Baerends, E. J. *Int. J. Quantum Chem.* **1988**, *33*, 87.
(114) Vosko, H. S.; Wilk, L.; Nussair, N. *Can. J. Phys.* **1980**, *58*, 1200.
(115) Becke, A. D. *Phys. Rev. A* **1988**, *38*, 3098.
(116) Perdew, J. P. *Phys. Rev. B* **1986**, *33*, 8822.
(117) Perdew, J. P. *Phys. Rev. B* **1986**, *34*, 7046.
(118) Becke, A. D. *J. Chem. Phys.* **1988**, *88*, 2457.
(119) Krijn, J.; Baerends, E. J. Fit functions in the HFS-method. Internal Report, Free University of Amsterdam, 1981.